Journal of Engineering Science and Technology
Vol. 19, No. 6 (2024) 2072 - 2090

DYNAMIC MODELLING AND THE OPTIMIZING OF DRIVING TORQUE CONCERNING 3-RRR PARALLEL ROBOT BASED ON NEWTON'S EULER FORMULA

SONG YANG[1,*], ZHEN LIU[1], RUI M. CHAI[2]

[1]Xi'an Research Inst. of Hi-Tech, No. 2 Tong Xin Road,
710025, Xi'an City, Shaanxi Province, China
[2]Xi'an North Electro-Optic Co., Ltd. No. 35 Changle Middle Road,
710043, Xi'an City, Shaanxi Province, China
*Corresponding Author: yangsong9209@163.com

Abstract

In recent years, a great number of studies have been conducted around the dynamic analysis of parallel robots. In these studies, kinetic equations are established by Lagrange formula, the principle of virtual work and other methods, among which Newton-Euler formula is rarely employed. Featured by clear physical process and available intermediate quantity, Newton-Euler formula was applied in this paper to model a 3-RRR parallel robot. First of all, a kinematic equation of the system was established based on the closed vector correlation, and the singularity was analysed. Subsequently, the Newton-Euler recurrence formula of a single branch chain was established, and three branch chains were closed in the end effector by virtue of the constraints, so as to obtain the closed chain kinetic equation. The modular structure is conducive to programming calculation and its popularization to other models. Then, numerical simulation was carried out on three driving torque distribution modes, and the results were compared and analysed. It is found that different driving torque distribution modes have their respective characteristics and advantages. Finally, forward dynamics verification of the model was carried out by MSC.ADAMS®.

Keywords: Dynamics, Kinematics, Newton-Euler formula, Parallel robot, Redundant actuation.

1. Introduction

Recently, with the rapid industrial development, serial robots have been applied to spraying, machining, welding, assembly and other fields more widely and maturely. But the open chain topological structure leads to the increase in error accumulation, poor accuracy and insufficient rigidity. In contrast, parallel robots are characterized by strong carrying capacity, high mechanical rigidity, high accuracy, fast response, strong positioning capacity, etc. and have been widely applied to aviation manufacturing, motion simulation, medicine, etc. at present [1-11]. However, due to small workspace, complex singularities in the space and dynamic coupling, the development of parallel robots has been restricted to some extent.

As everyone knows, the complex singularity problem is a characteristic of parallel robots. How to expand the workspace and avoid singularities in the workspace has always been an important research content in the studies on parallel robots. In general, singularities can be divided into the first kind of singularity and the second kind of singularity [12]. For the second kind of singularity, Jacobian matrix method, screw theory and exponential product method can be adopted for analysis, among which Jacobian matrix method is a common analysis method.

Near the singular configuration, the driver will be unable to bear the force or torque applied on the end effector. The rigidity, accuracy and other performance of the mechanism will get worse, and the mechanism will acquire uncontrollable degrees of freedom (DOF). In such case, the mechanism is extremely prone to getting out of control. Therefore, during the design and application of parallel robots, the singular configuration should be avoided, mainly the second kind of singularity.

The common methods for avoiding the second kind of singularity mainly include structure design method, path planning method and redundancy method [13-15]. Among them, redundancy method is proved to be an extremely effective way to avoid the second kind of singularity. The said method includes kinematical redundancy and actuation redundancy [16, 17]. Contrarily speaking, the actuation redundancy method can avoid the second kind of singularity without introducing new DOF, and also improve the dynamic performance of the mechanism [18, 19]. Thus, it is a highly effective method to avoid singularity.

There are numerous research methods for dynamic modelling of parallel robots, including Newton-Euler formula, Kane formula, Lagrange formula, etc. However, in order to obtain the kinetic equation of the system, many researchers choose Lagrange formula and the principle of virtual [20, 21], while only a few researchers adopt Newton-Euler formula for dynamic modelling of parallel robots [22]. Newton-Euler formula has some unique advantages in modelling, such as clear physical process, the availability of intermediate quantity, etc. These characteristics are of great significance for optimizing the torque distribution, improving the dynamic performance of parallel robots and reducing the acting force of robot joints in operation.

Parallel robots suffer from singularities during movement, which can affect their dynamic performance and even lead to failure. This paper aims to address this issue by introducing redundant drives to eliminate the singularities and adopting the Newton-Euler method to build the model, followed by optimization of the torque distribution to enhance the dynamic performance of the parallel robot and reduce the force on its joints during operation, which is of great significance for the reliability and safety of the robot.

In this paper, a planar 3-RRR redundant robot was studied, with the specific contents as follows: In Part I, a brief description of the model was made. In Part II, kinematic and singularity analysis of the mechanism was carried out, a kinematic model was established based on the closed vector correlation, and its workspace was analysed. Besides, singularity analysis of the mechanism was made by Jacobian matrix method. In Part III, dynamic modelling was conducted, and Newton-Euler formula was employed to establish the kinetic equation of open chain system. Three branch chains were made to converge on the end effector according to the closed chain constraints, and a complete kinetic equation of the system was established. In Part IV, numerical analysis was conducted under non-redundant drive and redundant drive modes respectively, and the kinematic performance under the two modes was compared and analysed.

In addition, numerical simulation and analysis were carried out on the following three driving torque distribution modes: (a) non-redundant driving torque; (b) driving torque under the minimum norm of internal force of the passive joint B_i in the redundant drive mode; (c) driving torque under the minimum power of active joint in the redundant drive mode. In Part V, the forward rigid body dynamics simulation was verified based on Adams software. In Part VI, the conclusion was drawn.

2. Model Description

Let A_i represent the active joint position of the ith branch chain and record its coordinate as (x_{Ai}, y_{Ai}) and its angle as α_i. Then let B_i represent the joint position at the end of driven link of the ith branch chain and record its coordinate as (x_{Bi}, y_{Bi}) and its angle as β_i. The end effector position is marked as P, with its coordinate recorded as (x_P, y_P), and it is expressed in the vector form as $\mathrm{X}_P = [x_P \quad y_P]^T$. Select a set of coordinates as the active joint position, i.e., $A_1(0,289)$, $A_2(250,-144)$ and $A_3(-250,-144)$. Figure 1 shows the 3-RRR redundant parallel robot.

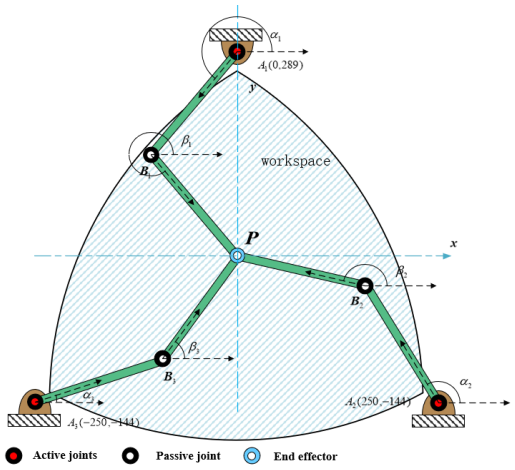

Fig. 1. 3-RRR redundant parallel robot.

When A_1,A_2,A_3 are selected as driving joints, a 3-RRR (R denotes the passive revolute joint and R denotes the active revolute joint) redundant parallel robot will

be formed. As the robot is of rotational symmetry, any two active joints can be selected as driving joints to form a 3-RRR non-redundant parallel robot.

3. Kinematic Analysis and Singularity Analysis

As shown in Fig. 1, the closed chain geometric equation of branch chain i can be written as

$$OP = OA_i + A_iB_i + B_iP \qquad i = 1,2,3 \tag{1}$$

Set out its scalar relations and process them to obtain

$$l_2 \cos\beta_i = x_P - x_{Ai} - l_1 \cos\alpha_i \tag{2}$$

$$l_2 \sin\beta_i = y_P - y_{Ai} - l_1 \sin\alpha_i \tag{3}$$

where, l_1 is the length of the driving rod, and l_2 is the length of the passive arm.

Square both sides at the same time to eliminateβ_i and obtain

$$(x_P - x_{Ai} - l_1 \cos\alpha_i)^2 + (y_P - y_{Ai} - l_1 \sin\alpha_i)^2 = {l_2}^2 \tag{4}$$

The expression of active joint angle can be acquired according to Eq.(4).

$$\alpha_i = a\tan 2\,(y_P - y_{Ai}, x_P - x_{Ai}) + \arccos\left(\frac{l_{AiP}}{2l}\right) \tag{5}$$

where,

$$l_{AiP} = \sqrt{(x_P - x_{Ai})^2 + (y_P + y_{Ai})^2}$$

Similarly, the expression of driven joint angle can be acquired.

$$\beta_i = a\tan 2\,(y_P - y_{Ai} - l_1 \sin(\alpha_i), x_P - x_{Ai} - l_1 \cos(\alpha_i)), \quad i = 1,2,3 \tag{6}$$

When the initial position of the end effector P is at the origin of coordinates, there are 6 possible initial configurations, and one of them is selected as the initial configuration for follow-up study.

3.1. Velocity and acceleration analysis:

For a parallel robot, to make its end effector move according to the planned trajectory, the input motion of active joints will have a quantitative relationship with the output motion of end effector, that is, inverse velocity Jacobian between the input and the output. Derive the closed chain equation (1) for time t to obtain:

$$\dot{X}_P = l_1\dot{\alpha}_1\tilde{E}l_{i1} + l_2\dot{\beta}_i\tilde{E}l_{i2} \tag{7}$$

where,$\dot{X}_P = [\dot{x}_P \quad \dot{y}_P]^T$ represents the velocity vector of the end effector.$\dot{\alpha}_i$ and $\dot{\beta}_i$ represent the angular velocity of active joint and driven joint respectively.

$\tilde{E} = \begin{bmatrix} 0 & -1 \\ 1 & 0 \end{bmatrix}$ is the planar cross operator of 2×2. $l_{i1} = [\cos\alpha_i \quad \sin\alpha_i]^T$ and $l_{i2} = [\cos\beta_i \quad \sin\beta_i]^T$ represent the unit direction vector of driving link and driven link of the ith branch chain respectively.

Premultiply Eq.(7) by ${l_{i2}}^T$ to obtain

$$l_1\dot{\alpha}_i {l_{i2}}^T\tilde{E}l_{i1} = {l_{i2}}^T\dot{X}_P \qquad (i = 1,2,3) \tag{8}$$

Further process Eq.(8) to obtain

$$\dot{\alpha}_i = J_{\alpha i}\dot{X}_P \tag{9}$$

where,$J_{\alpha i} = (l_1 {l_{i2}}^T \tilde{E} l_{i1})^{-1} {l_{i2}}^T$ is defined as the inverse velocity Jacobian matrix of active joint α_i;

The 3 branch chains can be uniformly expressed as the following matrix relation:

$$\dot{\alpha} = J_\alpha \dot{X}_P \tag{10}$$

where, $\dot{\alpha} = [\dot{\alpha}_1 \quad \dot{\alpha}_2 \quad \dot{\alpha}_3]^T$ represents the angular velocity vector of active joint, $\dot{X}_P = [\dot{x}_P \quad \dot{y}_P]^T$ refers to the velocity vector of the end effector, and $J_\alpha = [{J_{\alpha 1}}^T \quad {J_{\alpha 2}}^T \quad {J_{\alpha 3}}^T]^T$ is defined as the inverse angular velocity Jacobian matrix of active joint.

Solve the reciprocal of time based on Eq.(10) to obtain

$$\ddot{\alpha} = \dot{J}_\alpha \dot{X}_P + J_\alpha \ddot{X}_P \tag{11}$$

where,$\ddot{\alpha} = \left[\ddot{\alpha}_1 \quad \ddot{\alpha}_2 \quad \ddot{\alpha}_3\right]^T$ represents the angular acceleration vector of active joint, and $\ddot{X}_P = [\ddot{x}_P \quad \ddot{y}_P]^T$ refers to the acceleration vector of the end effector.

Similarly, in order to acquire the relation between the angular velocity of driven joint and the end operating platform, premultiply Eq.(7) by ${l_{i1}}^T$ to obtain

$$l_1 \dot{\alpha}_i {l_{i1}}^T \tilde{E} l_{i1} = {l_{i1}}^T \dot{X}_P - l_2 \dot{\beta}_i {l_{i1}}^T \tilde{E} l_{i2} \tag{12}$$

Process Eq.(12) to acquire

$$\dot{\beta}_i = J_{\beta i}\dot{X}_P \tag{13}$$

where, $J_{\beta i} = \left(l_2 {l_{i1}}^T \tilde{E} l_{i2}\right)^{-1} {l_{i1}}^T$ is defined as the inverse angular velocity Jacobian matrix of driven joint.

The 3 branch chains can be uniformly expressed as the following matrix relation:

$$\dot{\beta} = J_\beta \dot{X}_P \tag{14}$$

$\dot{\beta} = [\dot{\beta}_1 \quad \dot{\beta}_2 \quad \dot{\beta}_3]^T$represents the angular velocity vector of driven joint,

$J_\beta = \left[{J_{\beta 1}}^T \quad {J_{\beta 2}}^T \quad {J_{\beta 3}}^T\right]^T$ is defined as the inverse angular velocity Jacobian matrix of driven joint.

Solve the reciprocal of time based on Eq. (14) to obtain

$$\ddot{\beta} = \dot{J}_\beta \dot{X}_P + J_\beta \ddot{X}_P \tag{15}$$

where,$\ddot{\beta} = [\ddot{\beta}_1 \quad \ddot{\beta}_2 \quad \ddot{\beta}_3]^T$ represents the angular acceleration vector of driven joint, and $\ddot{X}_P = [\ddot{x}_P \quad \ddot{y}_P]^T$ refers to the acceleration vector of the end effector.

The angular accelerations of the active and passive links are determined by the planned angular speed and acceleration of the terminal executor P, and they are quantitatively related through the Jacobian matrix.

3.2. Analysis of center-of-mass velocity:

For branch chain i,

$$r_{Cai} = r_{Ai} + \frac{1}{2} l_1 l_{i1} \tag{16}$$

$$r_{Cbi} = r_{Ai} + l_1 l_{i1} + \frac{1}{2} l_2 l_{i2} \tag{17}$$

where, r_{Ai} represents the position vector of active joint support. r_{Cai} and r_{Cbi} respectively represent the center of mass position vector of driving link and driven link of the ith branch chain.

Derive Eqs. (16) and (17) for time t respectively to obtain

$$v_{Cai} = \frac{1}{2} l_1 \dot{\alpha}_i \tilde{E} l_{i1} \tag{18}$$

$$v_{Cbi} = l_1 \dot{\alpha}_i \tilde{E} l_{i1} + \frac{1}{2} l_2 \dot{\beta}_i \tilde{E} l_{i2} \tag{19}$$

where, v_{Cai} and v_{Cbi} respectively represent the centre of mass velocity vector of driving link and driven link on the ith branch chain.

Solve the first order derivative of time based on formulas (18) and (19) to acquire the centre-of-mass acceleration expressions of driving link and driven link respectively, as shown below

$$\dot{v}_{Cai} = \frac{1}{2} l_1 \ddot{\alpha}_i \tilde{E} l_{i1} + \frac{1}{2} l_1 \dot{\alpha}_i \tilde{E} \dot{l}_{i1} \tag{20}$$

$$\dot{v}_{Cbi} = l_1 \ddot{\alpha}_i \tilde{E} l_{i1} + l_1 \dot{\alpha}_i \tilde{E} \dot{l}_{i1} + \frac{1}{2} l_2 \ddot{\beta}_i \tilde{E} l_{i2} + \frac{1}{2} l_2 \dot{\beta}_i \tilde{E} \dot{l}_{i2} \tag{21}$$

where, $\dot{v}_{Cai}$ and $\dot{v}_{Cbi}$ respectively represent the centre of mass acceleration vector of driving link and driven link on the i^{th} branch chain.

Solve the first order derivative of time based on Eq.(1) and process it to obtain:

$$\begin{bmatrix} \dot{x}_P \\ \dot{y}_P \end{bmatrix} = \begin{bmatrix} l_1 \sin(\alpha_i) & l_2 \sin(\beta_i) \\ -l_1 \cos(\alpha_i) & -l_2 \cos(\beta_i) \end{bmatrix} \begin{bmatrix} \dot{\alpha}_i \\ \dot{\beta}_i \end{bmatrix} \tag{22}$$

Process Eq.(22) to obtain

$$\begin{bmatrix} \dot{\alpha}_i \\ \dot{\beta}_i \end{bmatrix} = \begin{bmatrix} -r_{ai} \cos\beta & -r_{ai} \sin\beta \\ r_{bi} \cos\alpha & r_{bi} \sin\alpha \end{bmatrix} \begin{bmatrix} \dot{x}_P \\ \dot{y}_P \end{bmatrix} \tag{23}$$

where, $r_{ai} = \frac{1}{l_1 \sin(\beta-\alpha)}$ and $r_{bi} = \frac{1}{l_2 \sin(\beta-\alpha)}$

3.3. Singularity analysis

Robot singularity refers to a specific point in the robot's workspace where the robot loses one or more degrees of freedom. In practice, when the tool centre of the robot enters or approaches a singular point, the robot may stop moving or move in an unexpected manner. Singularity occurs when the rank of the Jacobian matrix is less than the maximum rank that it can achieve in some configurations. When the determinant of the Jacobian matrix is zero, there exists a specific robot configuration that is singular.

As the singularity of parallel robot has a great influence on its working performance, the singularity under non-redundant drive and redundant drive modes is analysed respectively by matrix analysis below.

Premultiply Eq.(7) by $l_{i2}{}^{T}$ to obtain

$$l_1\dot{\alpha}_i l_{i2}{}^{T}\tilde{E}l_{i1} = l_{i2}{}^{T}\dot{X}_P \quad (i = 1,2,3) \tag{24}$$

Equation (24) can be utilized to obtain the mapping relationship between input and output:

$$J_{in}\dot{q}_{active} = J_{out}\dot{X}_P \tag{25}$$

where, $\dot{q}_{active}$ represents the angular velocity array of active joint; J_{in} and J_{out} are defined as the direct Jacobian matrix and indirect Jacobian matrix respectively. There are two drive modes in this paper, i.e., non-redundant drive and redundant drive, and the singularity under the two modes will be analysed respectively below.

3.3.1. Non-redundant drive

Due to the rotational symmetry of 3-RRR parallel robot, when A_1,A_2 are selected as driving joints, in Eq.(25),

$$\dot{q}_{active} = [\dot{\alpha}_1 \quad \dot{\alpha}_2]^T$$
$$J_{in} = diag(l_1 l_{12}{}^{T}\tilde{E}l_{11}, l_1 l_{22}{}^{T}\tilde{E}l_{21})$$
$$J_{out} = [l_{12}{}^{T} \quad l_{22}{}^{T}]^T$$

In this case, both the direct Jacobian matrix J_{in} and the indirect Jacobian matrix J_{out} are 2×2 square matrices. When the condition outlined below is met: $det(J_{in}) = 0$, Where $det(\cdot)$ represents the determinant of the matrix.

That is, when the condition $\beta_i - \alpha_i = k\pi \quad (i = 1,2; k = -1,0,1)$ is satisfied, the first kind of singularity will occur, and the end operating platform will reach the boundary of the theoretically reachable workspace.

When the condition outlined below is met: $det(J_{out}) = 0$, that is, when the condition $\beta_1 - \beta_2 = k\pi \quad (k = -1,0,1)$ is satisfied, the second kind of singularity will occur, and these singularities will exist inside the workspace.

3.3.2 Redundant drive

When A_1,A_2,A_3 are selected as driving joints to form the redundant drive mode, in Eq. (25),

$$\dot{q}_{active} = [\dot{\alpha}_1 \quad \dot{\alpha}_2 \quad \dot{\alpha}_3]^T$$
$$J_{in} = diag(l_1 l_{12}{}^{T}\tilde{E}l_{11}, l_1 l_{22}{}^{T}\tilde{E}l_{21}, l_1 l_{32}{}^{T}\tilde{E}l_{31})$$
$$J_{out} = [l_{12}{}^{T} \quad l_{22}{}^{T} \quad l_{32}{}^{T}]^T$$

In this case, the direct Jacobian matrix J_{in} is a 3×3 square matrix, and the indirect Jacobian matrix J_{out} is a 3×2 non-square matrix. Similar to the aforementioned method, if the first kind of singularity occurs, it is required to satisfy the condition $det(J_{in}) = 0$, which is the same as the result of non-redundant drive, i.e., the end operating platform reaches the boundary of the theoretically reachable workspace. If the second kind of singularity occurs, it is required to

satisfy the condition $rank(J_{out}) < 2$, that is, the rank of indirect Jacobian matrix J_{out} is reduced. But due to geometric constraints, J_{out} is always full-rank. Therefore, the second kind of singularity will not occur in redundant drive mode, and its workspace is as shown in the shaded area of Fig. 1, where there is no singularity.

4. Dynamic Modelling and Driving Torque Optimization

At present, there are a great number of dynamic modelling methods, including Lagrange equation method, Kane method, Newton-Euler method, etc. Most of them have ignored the intermediate process in order to facilitate the solution, thus simplifying the solution process of the kinetic equation of parallel robots to some extent. Therefore, many researchers choose energy method for solution, and only a few researchers adopt Newton-Euler formula. But Newton-Euler formula has some unique advantages, such as clear physical process, the availability of intermediate process quantity, etc. which are of great significance for the research on parallel robots.

Therefore, in this paper, Newton-Euler method was employed for dynamic analysis of 3-RRR parallel robot. As a total of 3 branch chains of the model converged to the central end effector, to facilitate the recursive analysis of internal force of the whole mechanism by Newton-Euler method, the whole parallel robot was firstly cut open along the passive joint and end effector, and applied with constraining force, as shown in Fig. 2. Then, recursive analysis was carried out on branch chains, and the recurrence formula of a branch chain was established. Finally, a complete dynamic model of the 3-RRR parallel robot was established on the basis of the closed chain constraint relationship.

Meanwhile, in order to simplify the model, it is assumed that all links and the end effector are made of the materials with uniform texture, and all joints are lightweight ideal bearings, i.e., with no mass, no friction, no clearance, etc.

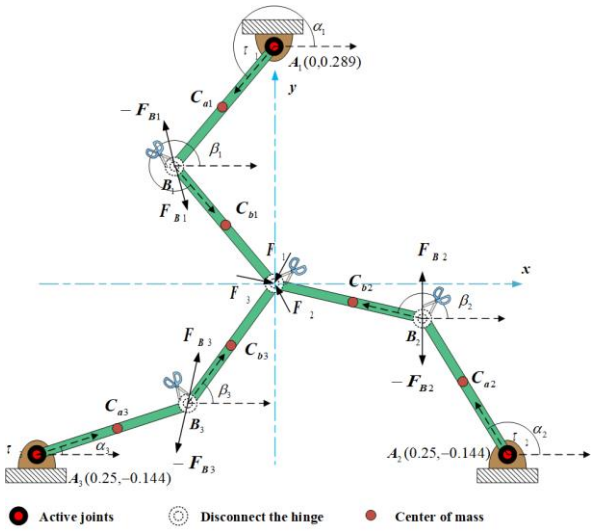

Fig. 2. Equivalent open chain system of 3-RRR parallel robot.

4.1. Newton-Euler recurrence formula on branch chain i

Newton-Euler method is a method used to build dynamic models, which is based on Newton's laws of motion and Euler's dynamics of rotation.

Set out Newton formula on the driven link:

$$F_{Bi} = F_i + m_2\dot{v}_{Cbi} \qquad i = 1,2,3 \tag{26}$$

where,F_{Bi} is the acting force of driving link A_i on the driven link B_i, and F_i is the acting force of driven link B_i on the end effector.

List the Euler formula on the driven link:

$$C_{bi}B_i \times F_{Bi} + C_{bi}P \times (-F_i) = I_b\dot{\beta}_i + \beta_i \times (I_b\beta_i) \qquad i = 1,2,3 \tag{27}$$

Substitute Newton recurrence Eq. (26) into Eq. (27) and eliminate F_{Bi} to acquire

$$G_iF_i = L_i \qquad i = 1,2,3 \tag{28}$$

where,

$$L_i = -C_{bi}B_i \times m_2\dot{v}_{Cbi} + I_b\dot{\beta}_i + \beta_i \times (I_b\beta_i) \qquad i = 1,2,3 \tag{29}$$

$$G_i = (C_{bi}B_i \times) - (C_{bi}P \times) \qquad i = 1,2,3 \tag{30}$$

Carry out recurrence further to the active joint to obtain the Euler formula on driving link:

$$A_iB_i \times (-F_{Bi}) + M_i = I_a\dot{\alpha}_i + \alpha_i \times (I_a\alpha_i) \qquad i = 1,2,3 \tag{31}$$

Similarly, substitute Newton Eq.(26) into Eq. (31) and carry out processing to obtain:

$$M_i = A_iB_i \times F_i + U_i \qquad i = 1,2,3 \tag{32}$$

where,

$$U_i = A_iB_i \times m_2\dot{v}_{Cbi} + I_a\dot{\alpha}_i + \alpha_i \times (I_a\alpha_i) \qquad i = 1,2,3 \tag{33}$$

$M_i = [0 \quad 0 \quad \tau_i]^T$is the torque acting on the active joint A_i.

4.2. Kinetic equation of closed chain system

Set out the specific forms of Eq.(28) in three branch chains

$$G_1F_1 = L_1, G_2F_2 = L_2, G_3F_3 = L_3 \tag{34}$$

Draw out the third line of the three formulas in (34) respectively and carry out processing to get

$$BF = C \tag{35}$$

where, $B = diag(B_1 \quad B_2 \quad B_3)$; $F = [F_1 \quad F_2 \quad F_3]^T$ is the resultant acting force of driven link on the end effector; $C = [C_1 \quad C_2 \quad C_3]^T$.

Set out the specific forms of Eq.(32) in three branch chains:

$$\begin{cases} M_1 = (A_1B_1 \times)F_1 + U_1 \\ M_2 = (A_2B_2 \times)F_2 + U_2 \\ M_3 = (A_3B_3 \times)F_3 + U_3 \end{cases} \tag{36}$$

As the parallel manipulator undergoes motion within the x-y plane, the third line of Eq.(36) is drawn out and the three branch chains are processed to get

$$\tau = DF + G \tag{37}$$

where, $\tau = [\tau_1 \quad \tau_2 \quad \tau_3]^T$ is the driving torque; $D = diag(D_1 \quad D_2 \quad D_3)$.

Combine formulas (35) and (37) and write them as follows:

$$\begin{bmatrix} B \\ D \end{bmatrix} F = \begin{bmatrix} 0_{3\times1} \\ \tau \end{bmatrix} + \begin{bmatrix} C \\ -G \end{bmatrix} \tag{38}$$

Since $\begin{bmatrix} B \\ D \end{bmatrix}$ is a 6×6 square matrix, Eq.(38) can be written as follows:

$$F = \begin{bmatrix} B \\ D \end{bmatrix}^{-1} \left(\begin{bmatrix} 0_{3\times1} \\ \tau \end{bmatrix} + \begin{bmatrix} C \\ -G \end{bmatrix} \right) \tag{39}$$

Supplement the intermediate constraint relationship

$$F_1 + F_2 + F_3 = m_3\ddot{X}_P \tag{40}$$

For the convenience of processing, Eq.(39) is written as follows

$$ZF = m_3\ddot{X}_P \tag{41}$$

where, $Z = [E_2 \quad E_2 \quad E_2]$, and E_2 is a 2×2 identity matrix.

Substitute Eq.(39) into Eq. (41) to obtain

$$Z \begin{bmatrix} B \\ D \end{bmatrix}^{-1} \left(\begin{bmatrix} 0_{3\times1} \\ \tau \end{bmatrix} + \begin{bmatrix} C \\ -G \end{bmatrix} \right) = m_3\ddot{X}_P \tag{42}$$

where, $H = Z \begin{bmatrix} B \\ D \end{bmatrix}^{-1}$.

$$H \begin{bmatrix} 0_{3\times1} \\ \tau \end{bmatrix} = m_3\ddot{X}_P - H \begin{bmatrix} C \\ -G \end{bmatrix} \tag{43}$$

Process the above formula to obtain

$$N\tau = m_3\ddot{X}_P - H \begin{bmatrix} C \\ -G \end{bmatrix} \tag{44}$$

where, $N = \begin{bmatrix} H_{14} & H_{15} & H_{16} \\ H_{24} & H_{25} & H_{26} \end{bmatrix}$.

When the system is under non-redundant drive mode, that is, the third line in equation (44) is zero, the equation is still applicable.

In order to facilitate the follow-up optimization and the solution of internal forces, the expressions of internal forces of the end effector and driven joint are set out as follows:

$$F_{Bi} = \begin{bmatrix} B \\ D \end{bmatrix}^{-1} \left(\begin{bmatrix} 0_{3\times1} \\ \tau \end{bmatrix} + \begin{bmatrix} C \\ -G \end{bmatrix} \right) + m_2\dot{v}_{Cbi} \tag{45}$$

4.3. Optimal distribution of driving torque

There are a number of ways to optimize the driving force. Considering the energy consumption of the robot, the minimum energy criterion is selected as the optimal criterion for distributing driving torques; considering the lifespan of various components, the minimum joint force criterion is chosen as the optimal criterion

for distributing driving torques. In this paper, the minimum joint internal force and active joint power consumption were selected for optimization analysis of the driving force [23].

Minimum Joint Internal Force: The driving torque is distributed based on the minimum Euclidean norm of joint internal forces F_{B1}, F_{B2} and F_{B3} on three driven joints B_1 B_2 and B_3, i.e.,

$$\tau_1 = min \sqrt{\sum_{i=1}^{3} \|F_{Bi}\|^2}.$$

Minimum Power Consumption: Considering the power utilization rate of the system, the working condition with the minimum energy consumption of the driving force of active joint is taken as the optimal criterion for driving torque distribution, that is,

$$\tau_2 = min \sqrt{\sum_{i=1}^{3} (\tau_i \alpha_i)^2}$$

5. Dynamic Analysis and Numerical Simulation

Dynamics simulation analysis of 3-RRR parallel robot was carried out based on the dynamic model established in this paper. First of all, the moving trajectory of the end effector P was given. Subsequently, the kinematic and dynamic performance in non-redundant drive and redundant drive modes were analysed under this trajectory. Finally, the following three driving torque distribution modes of the end effector under this trajectory were solved, compared and analysed: (a) non-redundant driving torque; (b) driving torque under the minimum norm of internal force of the passive joint B_i in the redundant drive mode; (c) driving torque under the minimum power of active joint in the redundant drive mode.

In this simulation, for the planned path, the point P of the end operating platform should move from point $(0,0)$ to point $(-14.42 \text{ mm}, 36.15 \text{ mm})$ in a spiral path within 0-0.5s. The graphical representations of Figs. 3 and 4 depict the corresponding trajectory, velocity, and acceleration profiles of point P.

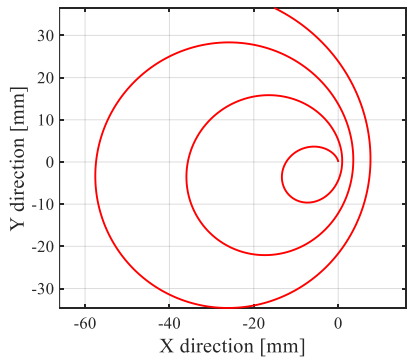

Fig. 3. Motion trajectory of Point P.

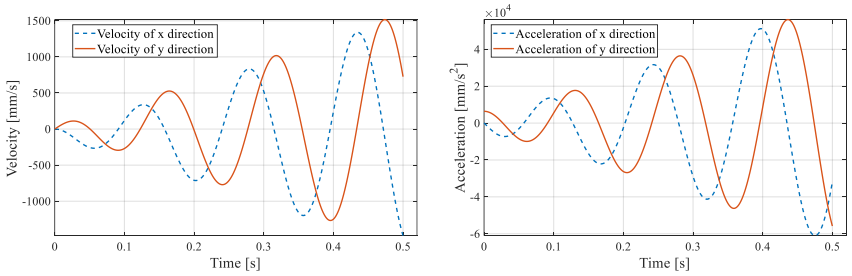

(a) **(b)**

Fig. 4. (a) Velocity of the end effector P, (b) Acceleration of the end effector P.

The parameters of a group of 3-RRR parallel robots are given as shown in Table 1. It is assumed that all links and the end operating platform are made of aluminium materials with uniform texture, and all joints are lightweight ideal bearings, i.e., with no mass, no friction, no clearance, etc.

Table 1. Parameters of 3-RRR parallel robot (Unit: mm).

l1	l2	Cross section A (mm^2)	Link thickness h	ρ (g/mm^3)
244	244	40	5	0.0027

As the 3-RRR robot is of rotational symmetry, A_1 and A_2 were selected as driving joints to form the non-redundant drive mode, and A_1, A_2 and A_3 were selected as driving joints to form the redundant drive mode.

According to the kinematic equation, numerical simulation was carried out to acquire the angular velocity and angular acceleration relationship of the active angle and driven angle under the redundant drive mode, as shown in Figs. 5 and 6.

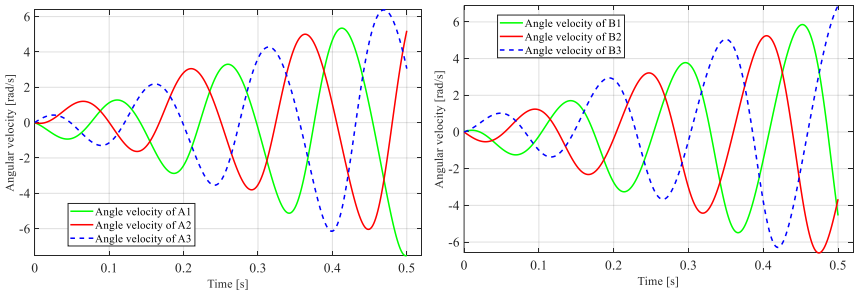

(a) **(b)**

Fig. 5. Under the redundant drive mode: (a) Angular velocity of active angle; (b) Angular velocity of driven angle.

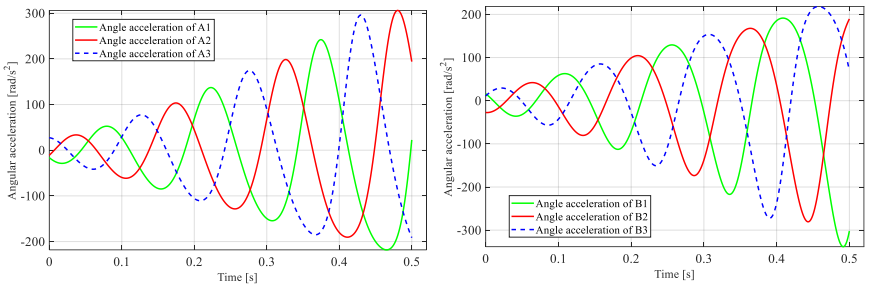

(a) **(b)**

Fig. 6. Under the redundant drive mode: (a) Angular acceleration of active angle; (b) Angular acceleration of driven angle.

According to different drive modes and optimization contents, the following three torque distribution modes were calculated respectively: (1) torque distribution in the non-redundant drive mode; (2) driving torque distribution under the minimum norm of internal force $\boldsymbol{F_{Bi}}$ of the passive joint B_i in the redundant drive mode; (3) driving torque distribution under the minimum norm of power consumption of the active joint in the redundant drive mode. The corresponding torque distribution conditions are as shown in Fig. 7:

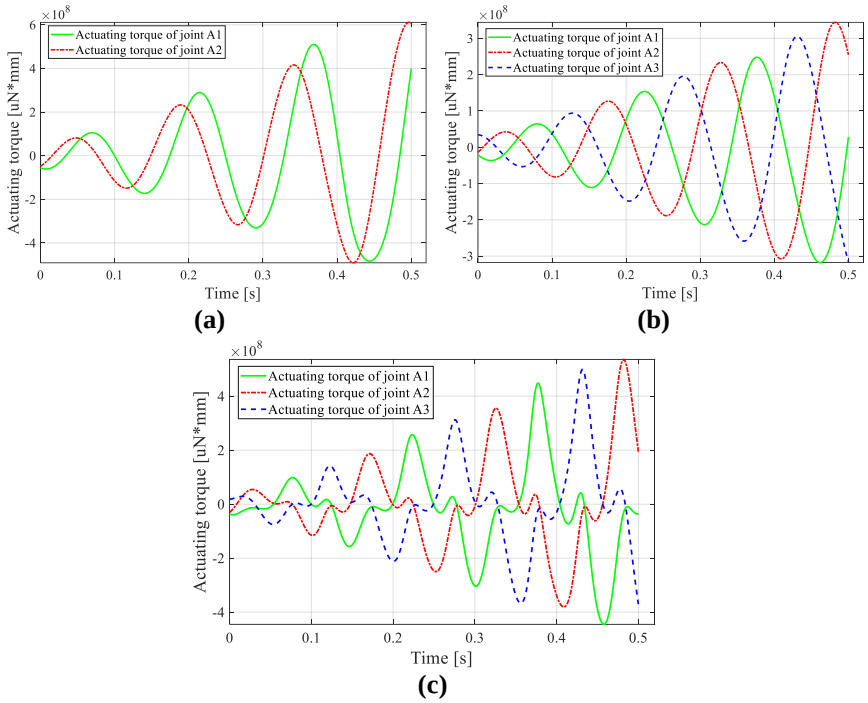

(a) **(b)**

(c)

Fig. 7. (a) Non-redundant driving torque; (b) Driving torque distribution under the minimum norm of internal force of the passive joint B_i in the redundant drive mode; (c) Driving torque distribution under the minimum power of active joint in the redundant drive mode.

It can be seen from the comparison of Fig. 7 that the peak value of driving torque in distribution mode 1 is the greatest, about $6 \times 10^8 \mu N \cdot mm$, while the driving torque in distribution mode 2 is the smallest, with its peak value of about $3 \times 10^8 \mu N \cdot mm$, which is only half of that in the non-redundant drive mode. The driving torque in distribution mode 3 is between the values in above two modes. Compared with the first two modes, its operation fluctuates to a certain extent and is not smooth enough. But the power of the active joint is the lowest in this distribution mode.

The internal force of passive joint B_i in driving torque distribution mode 2 is as shown in Fig. 8. The force on the passive joint is relatively balanced in this distribution mode, the interaction at the passive joint is small, and the peak values at the three joints are all about $1 \times 10^6 \mu N$ The internal force of passive joint B_i in driving torque distribution mode 3 is as shown in Fig. 9, and the peak values at three joints are all about $2 \times 10^6 \mu N$, which is about twice the internal force of passive joint B_i in driving torque distribution mode 2.

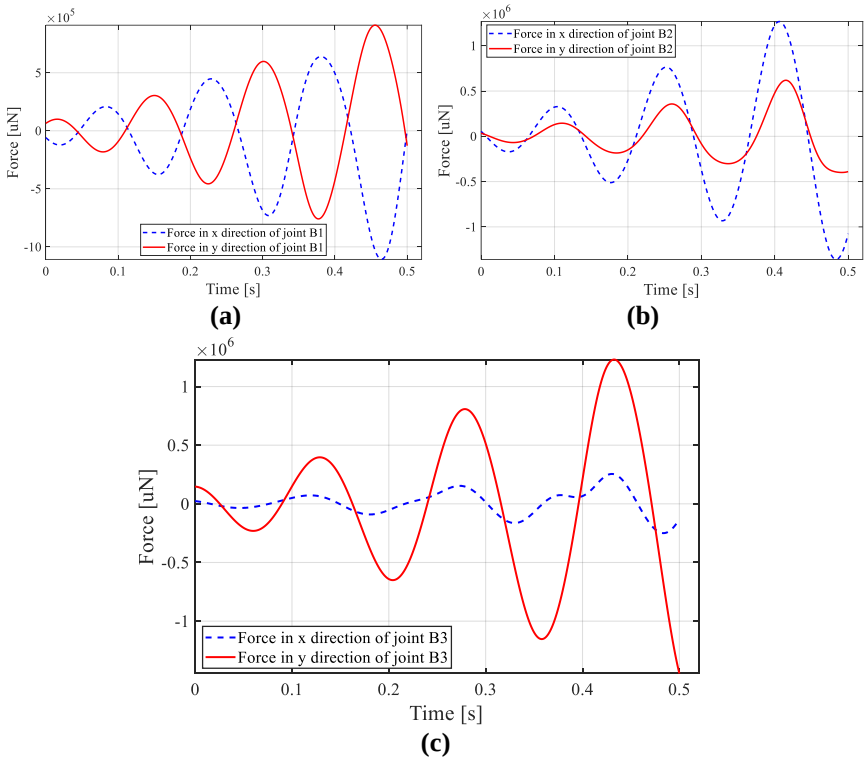

Fig. 8. Driving torque distribution mode under the minimum norm of internal force F_{Bi} of the passive joint in the redundant drive mode: (a) Internal force F_{B1} at the passive joint B_1; (b) Internal force F_{B2} at the passive joint B_2 (c) Internal force F_{B3} at the passive joint B_3.

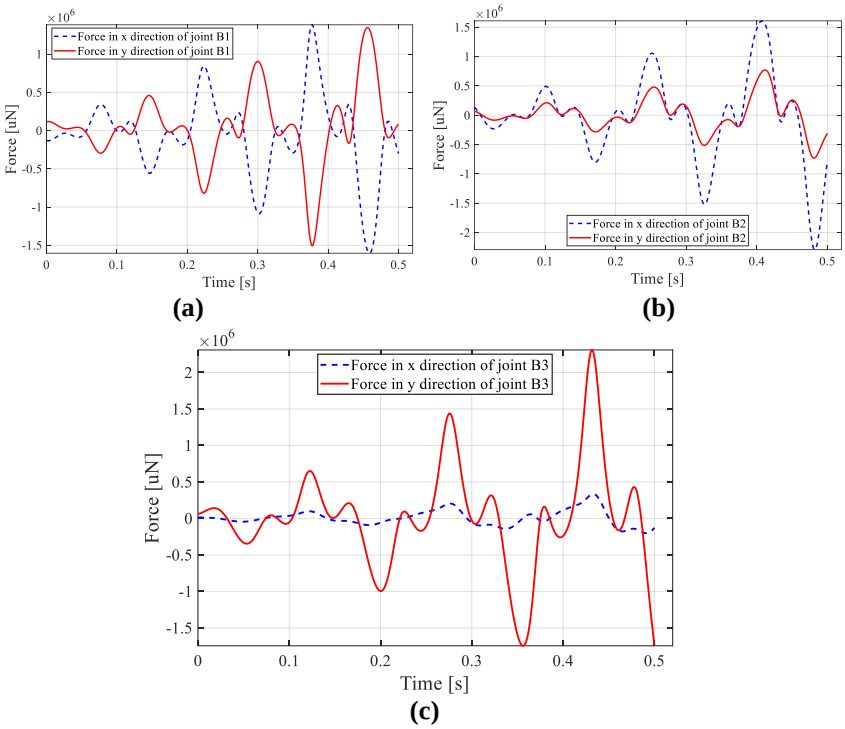

Fig. 9. Driving torque distribution under the minimum power consumption in the redundant drive mode: (a) Internal force F_{B1} at the passive joint B_1; (b) Internal force F_{B2} at the passive joint B_2; (c) Internal force F_{B3} at the passive joint B_3.

6. Forward Rigid Body Dynamics Simulation Based on Adams Software

Adams holds the top position as the most extensively utilized software for simulating mechanical systems globally [24]. By utilizing Adams, users have the ability to construct and evaluate a computer-based virtual prototype, thus realizing real-time online simulation and learning about the motion performance of complex mechanical system design. Firstly, a three-dimensional model of 3-RRR parallel robot was established in SolidWorks software, saved in the format of Parasolid and imported into Adams software. The gravitational force was set to zero, and various units were set as the established units to obtain the Adams software simulation model of virtual prototype.

Subsequently, the torque of 3 active joints under redundant drive obtained by numerical calculation was entered into Adams software in the form of test data as the feed-forward input of virtual prototype. Finally, the time was set as 0-0.5s, the number of steps as 1,000, and the analysis type as dynamic analysis. The simulation was started, and the simulation results were processed and sorted out.

In Adams software simulation, the motion trajectory of centre point P of the end operating platform is almost consistent with the trajectory planned in numerical simulation. Figure 10(a) shows the trajectory comparison results of point P in Adams simulation and numerical simulation. Compared with the planned trajectory

of point P, the displacement error in x direction is as shown in Fig. 10(b), with the maximum error of 0.4mm. The displacement error in y direction is as shown in Fig. 10(c), with the maximum error of 0.9mm. In Adams, the joints of virtual prototype model cannot be completely connected to the edge between links and the edge between the platform and links. Therefore, there is an error to some extent, and it is within the acceptable range. As such, it is verified that the rigid body dynamic model of 3-RRR parallel robot is of high accuracy and can provide theoretical support for rigid body dynamic modelling of parallel robots.

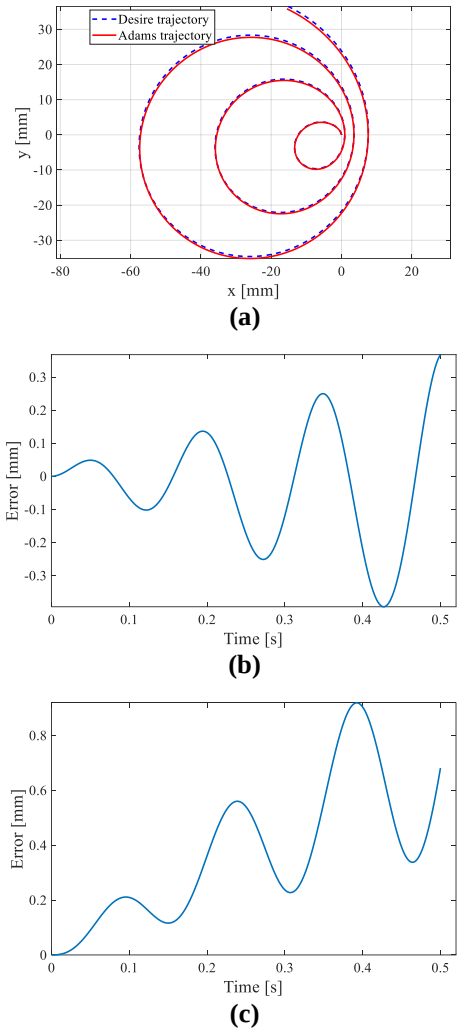

Fig. 10. Under the redundant drive mode: (a) Expected trajectory of the end effector P and the trajectory in Adams simulation; (b) Error between the expected trajectory of the end effector P and the trajectory in Adams simulation in x direction; (c) Error between the expected trajectory of the end effector P and the trajectory in Adams simulation in y direction.

7. Conclusion

In this paper, configurations of 3-RRR parallel robot are determined at first, and one set of the six possible initial configurations is selected as the initial configuration. Then, a complete dynamic model is established by kinematic and dynamic analysis of the model. On this basis, numerical analysis and driving force optimization are carried out. Finally, the model is verified in Adams. The specific work and conclusion are presented as follows:

- The model was subjected to a kinematic analysis, and a dynamic model of the system was established using the Newton-Euler method, which also yielded the internal forces at each joint for easy optimization of the force distribution.
- It is assumed that the constraints at the end effector and passive joint are removed, then the Newton-Euler recurrence formula of the ith branch chain is established. The internal forces of each joint, along with the angular speeds and angular accelerations of the links, are obtained through derivation, and these parameters are significant for the control and improvement of the dynamic performance of parallel robots. Subsequently, a complete closed kinetic equation is established in combination with the constraint equation. Modular structure is adopted in the whole modelling process, which is not only conducive to programming calculation, but also helpful for its popularization to other models.
- For solving the inverse kinetic equation, three driving torque distribution modes are employed, that is, (1) driving torque distribution mode in the non-redundant drive mode; (2) driving torque distribution mode under the minimum norm of internal force F_{Bi} of the passive joint B_i in the redundant drive mode; (3) driving torque distribution mode under the minimum norm of driving power of the active joint in the redundant drive mode. By comparing the numerical simulation results, it is found that the peak value of driving torque in mode 2 is half of that in mode 1. In addition, the ratio of three driving torques is more uniform, and the torque also changes with time more smoothly than that in mode 3. As such, the parallel robot moves more smoothly and has better dynamic characteristics. Moreover, this mode is subject to redundant drive design, which can help the parallel robot to successfully overcome the singularities. Furthermore, it is found through comparison that the peak value of internal force of driven joint in mode 2 is only about half of that in mode 3, and changes more stably. Therefore, through comprehensive consideration, mode 2 has a better dynamic performance, and in this mode, the internal force of driven joint changes more stably and is also smaller. However, in mode 3, under the minimum driving power of active joint, although the joint internal force increases, it does not increase significantly. Thus, this mode is of special advantages in controlling the input power and improving the power utilization rate. In addition to this, based on the internal forces already calculated for each link, the mode of force distribution can be optimized according to various needs, which is an advantage of modelling with the Newton-Euler method.
- Finally, by forward rigid body dynamics simulation through Adams software, the correctness and high accuracy of rigid body dynamic modelling of the parallel robot are verified, thereby providing theoretical support for rigid body dynamic modelling of parallel robots.

- The potential application fields of the parallel robot including fast packaging, fast sorting, high-speed motion simulation, etc. Future research plans will replace all rigid links with flexible ones to more realistically account for the flexibility of the robot's links and optimize accordingly.

Acknowledgments

The authors would like to appreciate the editors and the reviewers for their significant contributions to the improvement of the paper. Thanks to Xi'an Jiaotong University for their help in this study. In this paper, the MATLAB calculations and ADAMS dynamics simulations are completed in Xi'an Jiaotong University .©

References

1. Wang, M.; Liu, H.; Huang, T.; and Chetwynd, D.G. (2015). Compliance analysis of a 3-SPR parallel mechanism with consideration of gravity. *Mechanism and Machine Theory*, 84, 99-112.
2. Liang, D.; Song, Y.; Sun, T.; and Dong, G. (2016). Optimum design of a novel redundantly actuated parallel manipulator with multiple actuation modes for high kinematic and dynamic performance. *Nonlinear Dynamics*, 83, 631-658.
3. Zhang, H.; Fang, H.; Zhang, D.; Luo, X.; and Zou, Q. (2019). Forward kinematics and workspace determination of a novel redundantly actuated parallel manipulator. *International Journal of Aerospace Engineering*, 2019, 1-14.
4. Ren, B.; and Zhang, Z. (2021). Design of 4PUS-PPPS redundant parallel mechanism oriented to the visual system of flight simulator. *International Journal of Intelligent Robotics and Applications*, 5(4), 534-542.
5. Lin, R.; Guo, W.; and Cheng, S.S. (2022). Type synthesis of 2R1T remote center of motion parallel mechanisms with a passive limb for minimally invasive surgical robot. *Mechanism and Machine Theory*, 172, 104766.
6. Khalifa, A. et al. (2018). Development of a new 3-DOF parallel manipulator for minimally invasive surgery: 3-PUU parallel manipulator for MIS. *The International Journal of Medical Robotics and Computer Assisted Surgery*, 14(3), e1901.
7. Wu, J.; Gao, Y.; Zhang, B.; and Wang, L. (2017). Workspace and dynamic performance evaluation of the parallel manipulators in a spray-painting equipment. *Robotics and Computer-Integrated Manufacturing*, 44, 199-207.
8. Pedrammehr, S.; Nahavandi, S.; and Abdi, H. (2018). Closed-form dynamics of a hexarot parallel manipulator by means of the principle of virtual work. *Acta Mechanica Sinica*, 34(5), 883-895.
9. Thomas, M.J.; Joy, M.L.; and Sudheer, A.P. (2020). Kinematic and dynamic analysis of a 3-PRUS spatial parallel manipulator. *Chinese Journal of Mechanical Engineering*, 33(13), 1-17.
10. Chen, G.; Yu, W.; Li, Q.; and Wang, H. (2017). Dynamic modeling and performance analysis of the 3-PRRU 1T2R parallel manipulator without parasitic motion. *Nonlinear Dynamics*, 90(1), 339-353.

11. Cheng, C.; Xu, W.; and Shang, J. (2015). Optimal distribution of the actuating torques for a redundantly actuated masticatory robot with two higher kinematic pairs. *Nonlinear Dynamics*, 79, 1235-1255.
12. Zhou, Z.; and Gosselin, C. (2024). Simplified inverse dynamic models of parallel robots based on a Lagrangian approach. *Meccanica*. 59(4), 657-680.
13. Lin, J.; Han, H.; Yu, P.; Li, P.; Xu, Z.; and Wu, Q. (2024). Simplified dynamic characteristic analysis method for parallel manipulators with flexure hinges. *Nonlinear Dynamics*, 112(8), 6037-6059.
14. Hess-Coelho, T.A.; de Oliveira, É.L.; Orsino, R.M.M.; and Malvezzi, F. (2024). Modular modeling methodology applied to kinematically redundant parallel mechanisms. *Mechanism and Machine Theory*, 194, 105567.
15. Liu, Z.; Yang, S.; Ding, T.; and Chai, R. (2023). Dynamic modeling and performance analysis of a lower-mobility parallel robot with a rotatable platform. *Mathematical Biosciences and Engineering*, 20(2), 3918-3943.
16. Gosselin, C.; and Angeles, J. (1990). Singularity analysis of closed-loop kinematic chains. *IEEE Transactions on Robotics and Automation*, 6(3), 281-290.
17. Dash, A.K.; Chen, I.M.; Yeo, S.H.; and Yang, G. (2005). Workspace generation and planning singularity-free path for parallel manipulators. *Mechanism and Machine Theory*, 40(7), 776-805.
18. Wang, L.; Wu, J.; and Wang, J. (2010). Dynamic formulation of a planar 3-DOF parallel manipulator with actuation redundancy. *Robotics and Computer-Integrated Manufacturing*, 26(1), 67-73.
19. Yu, G.; Wu, J.; Wang, L.; and Gao, Y. (2020). Optimal design of the three-degree-of-freedom parallel manipulator in a spray-painting equipment. *Robotica*, 38(6), 1064-1081.
20. Baron, N.; Philippides, A.; and Rojas, N. (2019). A novel kinematically redundant planar parallel robot manipulator with full rotatability. *Journal of Mechanisms and Robotics*, 11(1), 011008.
21. Ebrahimi, I.; Carretero, J.A.; and Boudreau, R. (2007). 3-PRRR redundant planar parallel manipulator: Inverse displacement, workspace and singularity analyses. *Mechanism and Machine Theory*, 42(8), 1007-1016.
22. Yao, J.; Gu, W.; Feng, Z.; Chen, L.; Xu, Y.; and Zhao, Y. (2017). Dynamic analysis and driving force optimization of a 5-DOF parallel manipulator with redundant actuation. *Robotics and Computer-Integrated Manufacturing*, 48, 51-58.
23. Liang, D.; Song, Y.; Sun, T.; and Jin, X. (2018). Dynamic modeling and hierarchical compound control of a novel 2-DOF flexible parallel manipulator with multiple actuation modes. *Mechanical Systems and Signal Processing*, 103, 413-439.
24. Han, B.; Zhou, Y.; Zhang, J.; Xu, Y.; Yao, J.; and Zhao, Y. (2024). Kinematics and dynamics characteristics analysis of a double-ring truss deployable mechanism based on rectangular scissors unit. *Engineering Structures*, 307, 117900.